A New Semiautomated Detection Mapping of Flood Extent From TerraSAR-X Satellite Image Using Rule-Based Classification and Taguchi Optimization Techniques

Biswajeet Pradhan, Mahyat Shafapour Tehrany, and Mustafa Neamah Jebur

***Abstract*—Floods are among the most destructive natural disasters worldwide. In flood disaster management programs, flood mapping is an initial step. This research proposes an efficient methodology to recognize and map flooded areas by using TerraSAR-X imagery. First, a TerraSAR-X satellite image was captured during a flood event in Kuala Terengganu, Malaysia, to map the inundated areas. Multispectral Landsat imagery was then used to detect water bodies prior to the flooding. In synthetic aperture radar (SAR) imagery, the water bodies and flood locations appear in black; thus, both objects were classified as one. To overcome this drawback, the class of the water bodies was extracted from the Landsat image and then subtracted from that extracted from the TerraSAR-X image. The remaining water bodies represented the flooded locations. Object-oriented classification and Taguchi method were implemented for both images. The Landsat images were categorized into three classes, namely, urban, vegetation, and water bodies. By contrast, only water bodies were extracted from the TerraSAR-X image. The classification results were then evaluated using a confusion matrix. To examine the efficiency of the proposed method, iterative self-organizing data analysis technique (ISODATA) classification method was applied on TerraSAR-X after employing the segmentation process during object-oriented–rule-based method, and the results were compared. The overall accuracy values of the classified maps derived from TerraSAR-X using the rule-based method and Landsat imagery were 86.18 and 93.04, respectively. Consequently, the flooded locations were recognized and mapped by subtracting the two classes of water bodies from these images. The acquired overall accuracy for TerraSAR-X using ISODATA was considerably low at only 57.98. The current research combined the methods and the optimization technique used as an innovative flood detection application. The successful production of a reliable and accurate flood inventory map confirmed the efficiency of the methodology. Therefore, the proposed method can assist researchers and planners in implementing and expediting flood inventory mapping.**

***Index Terms*—Flood detection, GIS, Landsat, remote sensing, rule-based classification, Taguchi, TerraSAR-X.**

I. Introduction

APPROXIMATELY 4% of the land on the planet is covered by wetland ecosystems [1]. Most of these wetlands are floodplain and are located in tropical countries [2]. Every year, floods occur with increasing frequency and heavily damage lives and properties [3]. Floods can be managed efficiently through flood susceptibility, hazard, and risk mapping [4], [5] which is based on the identification of flooded areas [6]. Moreover, the reliability of a flood inventory map directly influences the generation of susceptibility and hazard maps [7]. Therefore, the method used to determine flood locations should be accurate. Flood detection analysis should also be rapid [8] because floods can subside quickly in an inundated area. Thus, researchers have limited time with which to map all of the locations. Fieldwork is unsuitable for such analysis given on-site challenges and difficulties [9]. It is time-consuming and costly, which is not practical for real-time studies [10]. Flood happens over a large area, thus making it difficult to reach all those areas as they will not stay for long duration [11]. Furthermore, traditional hydrological methods, such as gauge and discharge measurements, have some weak points to monitor and map flood locations because of the temporal and spatial heterogeneity of large wetlands [1]. The launch of various satellites and sensors has revolutionized the monitoring, evaluation, and prediction of natural disasters [12]. Moreover, flood detection has improved considerably because of the availability of multitemporal data, the increased spatial resolution, the development of change detection algorithms, and the incorporation of remote sensing techniques [13].

Visual interpretation is a popular method to detect flood locations. Reference [14] investigated the efficiency of this method using European remote sensing satellite data. The flood boundary was derived using automatic classification techniques. The results showed that visual interpretation is more accurate than satellite analysis. However, this finding is attributed to the poor resolution of the satellite data and the limitation of the technology and of computing software at the time. The recent access to a wide range of software, very high resolution satellite

Manuscript received September 21, 2015; revised January 7, 2016; accepted March 1, 2016. Date of publication April 4, 2016; date of current version May 24, 2016. This work was supported by the Ministry of Higher Education Research Project under Flood Disaster Management (project number: FRGS/1/2015/STWN06/UPM/02/1) with vote number 5524687 and also by the UPM University Research Grant (05-01-11-1283RU) to stimulate research under the RUGS scheme with project number 9344100.

B. Pradhan is with the Department of Civil Engineering, Geospatial Information Science Research Center, Faculty of Engineering, Universiti Putra Malaysia, 43400, Serdang Selangor Malaysia and also with the Department of Geoinformation Engineering, Choongmu-gwan, Sejong University, Seoul 05006, South Korea (e-mail: biswajeet24@gmail.com; biswajeet@lycos.com).

M. S. Tehrany and M. Neamah Jebur are with the Department of Civil Engineering, Geospatial Information Science Research Center, Faculty of Engineering, Universiti Putra Malaysia, 43400, Serdang Selangor Malaysia.

Digital Object Identifier 10.1109/TGRS.2016.2539957

imagery, and active and passive sensors facilitate the collection of data and the analysis and mapping of flood events within a few hours [15]. By contrast, the visual interpretation of satellite images is a time-consuming, inaccurate, and costly method. It is based on expert knowledge; therefore, it can be erroneous [16].

All of the optical images are unsuitable for flood detection applications [6], [17] because clouds usually cover the sky during a flood event, thereby limiting the observational capability of these optical sensors. Some of these sensors are incapable of penetrating the cloud cover, and they are highly affected by weather conditions. Thus, they have been replaced by active sensors, which are unaffected by sun illumination and atmospheric conditions [18]. Moreover, synthetic aperture radar (SAR) signals can penetrate vegetation and forest [19]. These sensors can operate both day and night and can highlight different aspects of a single terrain because of their single- or multipolarized capability. Furthermore, the flooded areas under vegetation can also be detected using specific SAR imageries [20]. Therefore, SAR imagery has much potential application in flood studies [21].

Researchers have assessed various techniques to map flooding events, and each technique has its pros and cons [18], [22] and [23]. For instance, the threshold segmentation algorithm or histogram thresholding is a simple but widely used and effective method to generate a binary image [22]. Reference [24] utilized this algorithm to map the extent of flooding in the Dongting Area of Hunan Province based on RADARSAT-1 imagery. Reference [1] mapped flood locations by a split-based automatic thresholding procedure on high-resolution TerraSAR-X data of southwest England, particularly at the River Severn, U.K. They stated that object-based context-sensitive thresholding is proven superior to pixel-based context-insensitive procedures owing to the addition of spatial information to the pure spectral information derived from histogram thresholding. The effectiveness of thresholding procedures for floodplain recognition with SAR sensors depends on the contrast between the flooded and nonflooded regions. Therefore, thresholding is sensitive to low-contrast images. However, this method is limited because it is tailored to each satellite scene, i.e., it is usually based on visual interpretation. Moreover, its procedure is manual and time-consuming [22]. The extent of flooding in an area can also be mapped by active contour modeling. Reference [23] applied this method to single-frequency and single-polarization SAR images to map the flood locations in Thames, which is west of Oxford, U.K. This method is advantageous because it limits the noise caused by SAR speckle. However, this method can only be used by a researcher with *a priori* knowledge of the statistical properties of images. Moreover, the method is hindered by local minima and is inaccurate when the initial selected contour is simple or is far from the object boundary.

Flood areas can be extracted from multipass SAR data through amplitude change detection techniques or the generation of a coherence map [25]. The amplitude change detection method compares two SAR images of the same scene: one captured prior to flooding and the other during or immediately after the event. Subsequently, the water-filled zones can be detected by determining the regions with reduced backscatter. However, amplitude change detection techniques are limited by their difficulty and by the significant amount of time required to classify at least two SAR data [25]. SAR interferometry should be conducted to produce a coherence map; however, this technique is often difficult to understand and interpret [26]. The generation of a coherence map is also complex and disadvantageous; for instance, it requires ground data and two precisely coregistered SAR images [27]. The ground data distinguish flooded areas from other low-coherence zones.

The SAR backscatter model from a river flood assumes that the water surface is smoother than the adjacent land and is a specular reflector that reflects radiation from a sensor. Therefore, the water appears darker than the land [23]. Paddy fields, part of the mountain facing away from the SAR sensor, and all water bodies also appear dark or black in radar imagery [6]. Therefore, we must develop a method that can discriminate between flooded areas and other objects. The current research aims to overcome some of the drawbacks of the existing methods and to establish a reliable and precise technique to detect flood locations. We aim to apply change detection without requiring two SAR images; instead, we utilize the SAR imagery captured during flooding because it can penetrate cloud cover and record all of the objects on the terrain surface.

Furthermore, a cloud-free Landsat image recorded prior to flooding was used, as the free Landsat data can reduce the required budget for the project and provide the required information under proper weather conditions. It is a well-known fact that various features appear dark in SAR imagery, such as building roofs, paddy fields, and water bodies. These features are discriminated using the object-oriented rule-based classification method. This method considers other object characteristics, such as texture and shape [28]. Therefore, this procedure involves two steps: 1) recognizing water versus nonwater regions before and during flooding and 2) comparing the regions categorized as water or nonwater before and during flooding to detect flooded areas.

II. Study Area and Data Used

In Malaysia, the Kuala Terengganu area has undergone much flooding over the last decade. Therefore, it was selected as the study area, in which the efficiency of the proposed method can be evaluated with respect to flood location detection (Fig. 1). Terengganu is situated in Peninsular Malaysia and is bordered by the South China Sea in the east. On November 27, 2009, a disastrous flood struck this area as a result of heavy precipitation. Therefore, this research utilized two data sources: TerraSAR-X imagery captured during flooding and Landsat imagery recorded during a nonflood instance. The applied SAR data were collected by a TerraSAR-X satellite on November 27, 2009, using HH polarization, single look, and 3 m of spatial resolution. Furthermore, the data were composed of stripmap modus and short TSX-1 images with 16-b radiometric resolution. HH polarization data are less affected by the variations in the roughness of water surfaces as caused by wind or vegetation than other polarization types [1]. On October 21, 2009, Landsat imagery with a spatial resolution of 30 m was acquired. The image was obtained from path 126 and row 56. However, its spatial resolution was enhanced after pan-sharpening, which is described in the section on preprocessing.

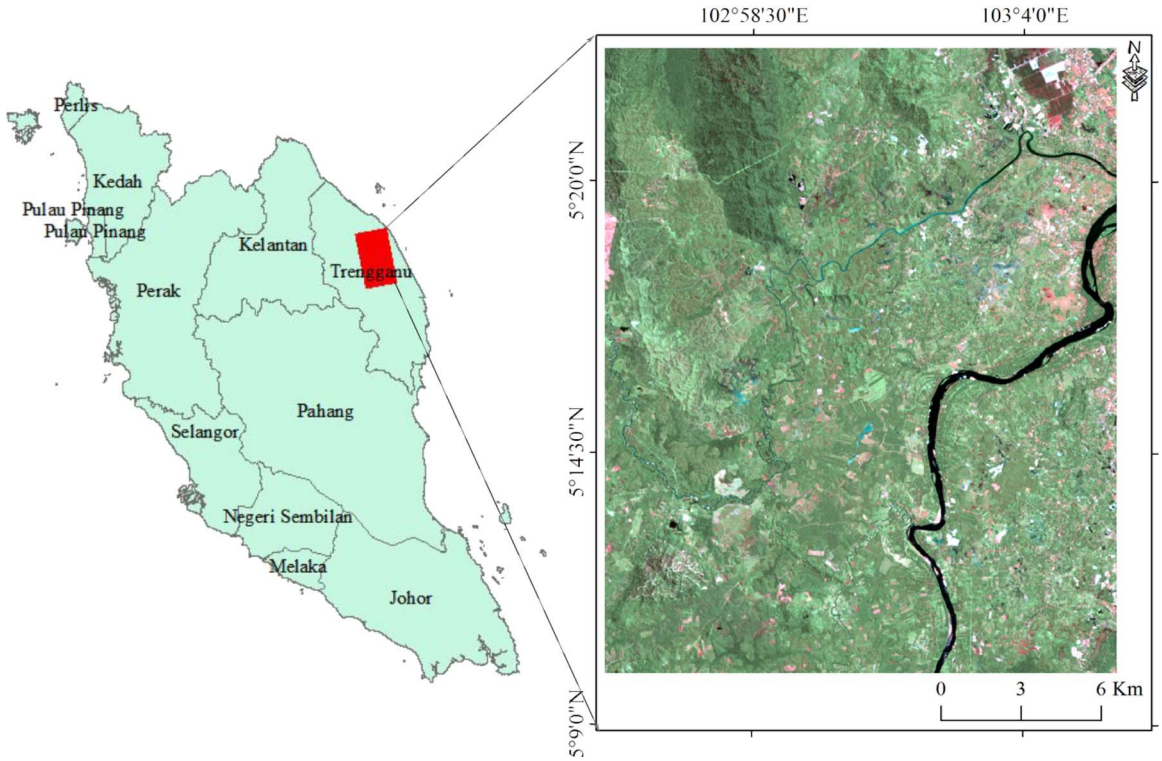

Fig. 1. Study area. (Left image) Malaysian states and (right image) Landsat imagery.

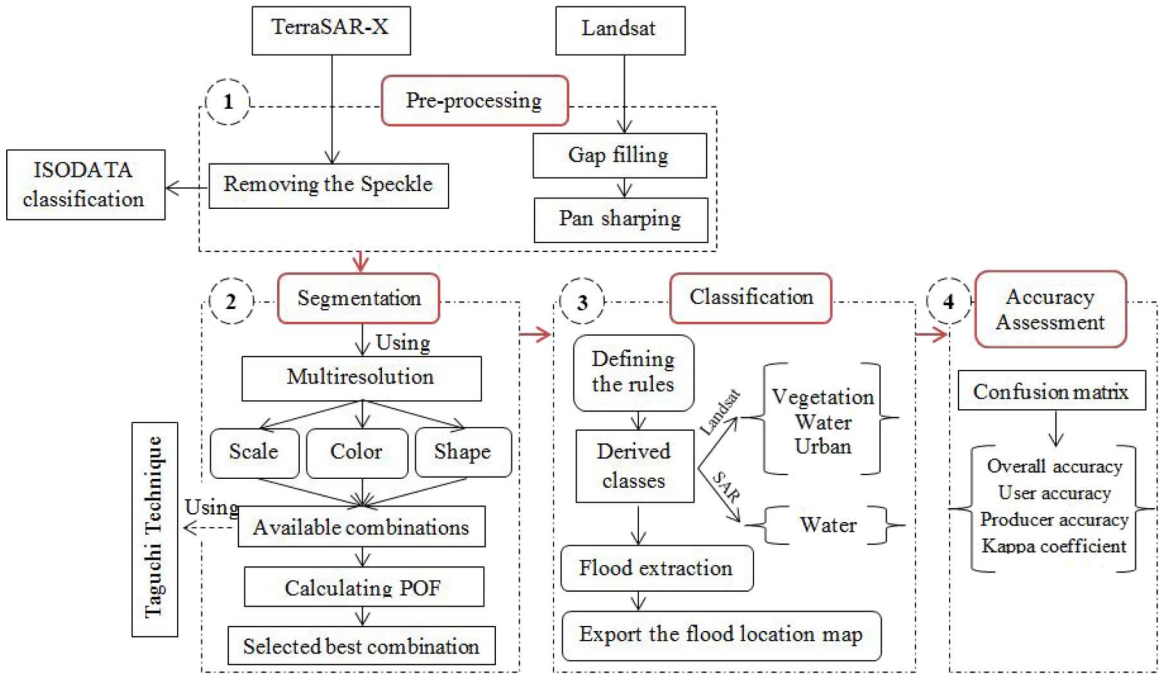

Fig. 2. Methodology flowchart.

III. Methodology

The general methodology implemented in this study is shown in Fig. 2. In the first stage, preprocessing was done for both images of Landsat and TerraSAR-X. Speckles were removed from TerraSAR-X using ISODATA method. Gap filling and pan-sharpening were applied for Landsat imagery in order to solve the problem of gaps in Landsat and increase the spatial resolution of this data. In order to perform object-oriented rule-based classification schemes, two main steps should be done. The first stage is segmentation, which defines the boundary of the objects. Here, Taguchi optimization technique was used in order to find the optimum segmentation combination. In the second stage, rules were defined, and classification was done based on the derived rules. Three classes of vegetation, water,

and urban were produced using the Landsat image. Similarly, TerraSAR-X was classified into two classes of water and nonwater bodies. By subtracting the two classes of water bodies from Landsat and TerraSAR-X, flooded areas were extracted. As a last step, validation was done using a confusion matrix, and reliability of flooded area map was assessed. Each stage is detailed in the succeeding sections.

A. Preprocessing

The original images must be preprocessed to generate reliable and precise outcomes. The gaps in Landsat imagery must be filled, and the image must undergo pan-sharpening. However, the Landsat 7 scan line corrector tool, which was designed to correct the undersampling of the primary scan mirror, failed to work in 2003. This increased scan gap induced a loss of approximately 22% of Landsat ETM+ information. Nonetheless, the gaps can be filled through numerous methods. The current study applied the local linear histogram matching method because it is often used by various researchers due to its highly accurate results [29], [30]. Reference [29] stated that the local linear histogram method is very simple and easy to implement and can resolve many of the missing-data problems. As stated in Section II, the Landsat imagery used in the current research was captured on October 21, 2009. The local linear histogram matching method filled the scan gap in the Landsat imagery obtained on August 18, 2009. To do so, the precise information on the available pixels and the pixels that should be filled must be determined. A scan gap mask was produced for each band that displays existing data as 1 and that denotes the missing data in the scan gap and areas to be filled by 0. Once the gaps were recognized, the linear histogram matching detected linear transformation in the images. Moreover, the Landsat imagery was pan-sharpened using the Gram-Schmidt (GS) spectral sharpening method [31]. The spatial resolution of the Landsat image was 30 m; however, this method can improve this spatial resolution by merging the high-resolution pan image with the bands of low spatial resolution [32]. Therefore, the spatial resolution of Landsat was enhanced to 15 m after pan-sharpening.

Speckles should be removed from the TerraSAR-X image using appropriate filters [33]. Filters such as Lee, Frost, and mean can suppress and smooth out the speckle effect [6]. However, each filter performs differently; consequently, not all are equally appropriate. A filter should not distort and degrade the inherent texture of the image. Thus, some of the filters were evaluated based on signal-to-noise ratio (SNR). Based on the visual interpretation and SNR values acquired in the current research, the Frost filter was better than the other filters. It accurately displayed the study area with low noise and no blurring effect. A 4×4 window Frost filter was therefore utilized to remove the speckle from TerraSAR-X imagery [6].

B. Rule-Based Classification

The classification techniques that are used to classify very high resolution optical images, including those of urban areas, are often unadaptable for SAR data. This unadaptability may be attributed to the spatial heterogeneity of urban areas. Therefore, the more advanced object-oriented rule-based method was used to classify the TerraSAR-X data. The rule-based classification method was also applied in Landsat imagery classification because of its efficiency [34]. Object-oriented classification is based on objects rather than on pixels using additional information, such as the texture and color of the objects [35], [36]. Using this additional information, object-oriented classification recognizes features such as floods more effectively than pixel-based techniques. This method applies expert rules in classification and suitably extracts the spectral family of signatures for a specific class and the spectral overlap among classes (e.g., floods have spectral characteristics that are similar to rivers and paddy fields), which is induced by restrictions in spectral resolution and bandwidth [37]. Nonetheless, a researcher can set comprehensive rules using additional information on spectral, spatial, textural, and contextual factors [38]. Object-oriented classification can also be implemented using different software, including eCognition, ERDAS Objective, and Envi Zoom. The current research utilized ENVI software because it is proficient in such applications and contains the appropriate analysis tools. Moreover, this method involves two main steps, namely, segmentation and proper definition of rules [38].

1) Segmentation Using the Taguchi Technique: In object-oriented classification, parameters such as scale, color, shape, and segments should be defined properly to recognize flooded areas. Segmentation is the first stage in object-oriented analysis, and it partitions an image into nonoverlapping regions [39]. SAR imagery often varies little in terms of mean amplitude among different types of land use/cover (LULC) [40]. However, SAR amplitude fails to differentiate among different features and LULC types strongly. As a result, texture has been considered as the main segmentation parameter in SAR imagery classification under numerous applications [41]. Segmentation precision significantly influences the quality of the final classified map. Therefore, this study used the multiresolution segmentation algorithm. It began with one pixel and progressed until all of the criteria were fulfilled [39]. This type of segmentation was achieved through parameters such as scale, color, and shape, which generate 243 combinations for segmentation. However, the effects of each combination are time-consuming to evaluate. Hence, an appropriate optimization technique should be developed to reduce the number of examinations and thus accelerate segmentation and classification. In line with this requirement, the Taguchi technique can obtain the optimum combination of segmentation parameters [39]. Reference [39] used this method to optimize pixel-based and object-oriented classification in mapping the landslide locations in Kermanshah City, Iran. Their research investigated and confirmed the efficiency of this method. Therefore, the current study aims to utilize this technique to optimize the segmentation parameters. Taguchi tables facilitate easy and stable experimental designs. Therefore, only 25 experiments are selected for assessment by the Taguchi method in terms of the three segmentation parameters. Moreover, the plateau objective function (POF) was measured for each test to evaluate segmentation precision in each of the 25 experiments. POF is a combination of a spatial autocorrelation index and a variance indicator. Precise segmentation is represented by a high POF. More information about POF can be obtained from [39].

TABLE I
DEFINED RULES FOR TERRASAR-X

Classes	Rules
Water bodies	25.78145 < HH band < 100.39737 9679.55415 < Area < 3030705 160.43092 < Texture variance < 1500
Non water bodies	HH band > 100.39737 Area > 3030705 Texture variance > 1500

To apply the general steps in the Taguchi method, the following steps were performed. 1) The process objective was determined in the beginning. This step entails defining the possible values of a particular parameter for the process. 2) The parameters that can influence the process were then defined. These parameters (scale, color, and shape) exhibit variable values that can affect performance; thus, the level should be defined by the user depending on the parameter's effect on the process. For instance, a scale value can vary from 0.1 to 1.0. When the level increases, the number of experiments to be conducted will be increased as well. 3) An orthogonal array was created to design the condition and determine the number of experiments. Selecting the orthogonal array depends on the number of levels and the number of parameters. 4) The experiments were then applied after the appropriate array had been selected. The effect of each parameter on the performance was then measured.

The loss function can be calculated as follows [42]:

$$l(y) = k_c(y - T)^2 \tag{1}$$

where T is the target value of y and the measured value y is a loss function. K_c is the constant in the loss function that can be calculated by considering the acceptable interval as follows:

$$k_c = \frac{C}{\Delta^2} \tag{2}$$

where C is the loss associated with sp limit and Δ is the deviation of the specification from the target value. When whole parameters that affect the process are defined, the level of each parameter should also be defined. The level refers to the probable value of each parameter in terms of maximum, minimum, and current values. In the case of a big gap between the minimum and maximum values of a specific parameter, additional levels are added to that parameter. The proper array was selected after the number of parameters and levels have been defined. A constant array was found for the Taguchi method. Each array can be selected depending on the parameters and levels. Table I was created using an algorithm of Taguchi. In the case of three parameters and two levels, L25 array was selected. The array assumes that the number of levels is equal for each parameter. Otherwise, the assumption will be based on the highest value.

2) Rule Definition: Rule-based classification aims to enhance feature classification precision. This method can reduce confusion errors among spectrally similar categories [43]. Moreover, a user can create and flexibly manipulate rules until the best classification results are obtained. The necessary rules were manually defined according to the segment attributes of both images. Tables I and II list the rules defined for the Landsat and TerraSAR-X imagery in the current research.

TABLE II
DEFINED RULES FOR LANDSAT

Classes	Rules
Water bodies	21.952460020 < NIR < 100.23437 18.36103 < SWIR < 86.36934 42.50064 < Texture variance < 1416.79126 NDVI < 1
Vegetation	NDVI > 0.2 109.68319 < NIR < 171.34019 84< RED < 87
Urban	-0.9 <NDVI < 0.2 181.003616 < Blue < 249.377014 129.782043< SWIR < 154.986801

C. Iterative Self-Organizing Data Analysis Technique (ISODATA) Classification

Another classification method was used for comparison with the acquired results to evaluate the efficiency of the proposed rule-based method. ISODATA is one of the most popular classification algorithms in image processing that requires few parameters, such as the number of classes to be derived, the number of iterations, and the threshold value [44]. In the current research, the algorithm was set to 10–20 classes, with a threshold of 5% and 1 iteration. ISODATA is an unsupervised statistical classification technique that produces a well-defined pixel or object classification. It entails assigning each pixel or segmented object to a specific class. Supervised classification methods require the user to define the characteristics of the classes prior to classification; unsupervised methods rely on the classification process itself to define the classes [45]. Unsupervised classification techniques create natural groupings of data in attribute space that can be used to obtain insight into the data structure. The ISODATA method is mostly used for satellite image classification. Spectral reflectance from different bands is used to find classes in multidimensional attribute space. The classification outcome should be analyzed by the user who has knowledge and experience of the features. In certain cases, the program assigns data to the classes that they do not really belong to [46]. The reason is that ISODATA is not very robust compared to other advanced classification techniques such as the rule-based method. It is unsupervised, and all of the decision was made based on spectral information. Hence, it is possible that some pixels are classified wrongly.

D. Validation

The accuracy of the generated flood inventory map can be determined based on the completeness of the map and the precision of the information shown [47]. The efficiency and the quality of the generated inventory map can be assessed using various methods. A popular method involves the development of a confusion matrix [48], [49]. The ground truth data for TerraSAR-X were collected from field survey from November 27 to 29, 2009. The number of locations that were used to perform accuracy assessment was 105, which were collected by GPS during field surveying. During the surveying, the boundaries of the flooded areas were measured. The number of the observed locations varies based on the area of the flood, where bigger areas had more observation compared to the small ones. However, the 105 sites represent the flood events rather than the number of the observation. Regarding the Landsat

TABLE III
L_{25} ORTHOGONAL ARRAY AND POF FOR SEGMENTATION PROCESS WHERE L REPRESENTS THE LEVEL WHICH REFLECTS THE NUMBER OF THE EXPERIMENTS

TerraSAR-X image							Landsat image						
L25 (Combination of different levels)			Scale	Color	Shape	POF	L25 (Combination of different levels)			Scale	Color	Shape	POF
1	1	1	20	0.1	0.1	0.705	1	1	1	20	0.1	0.1	0.672
1	2	2	20	0.3	0.3	1.176	1	2	2	20	0.3	0.3	1.081
1	3	3	20	0.5	0.5	1.050	1	3	3	20	0.5	0.5	1.034
1	4	4	20	0.5	0.5	0.914	1	4	4	20	0.5	0.5	1.285
1	5	5	20	0.9	0.9	1.113	1	5	5	20	0.9	0.9	0.896
2	**1**	**2**	**40**	**0.1**	**0.3**	**1.310**	2	1	2	40	0.1	0.3	1.138
2	2	3	40	0.3	0.5	0.870	2	2	3	40	0.3	0.5	0.857
2	3	4	40	0.5	0.5	0.822	2	3	4	40	0.5	0.5	1.144
2	4	5	40	0.5	0.9	0.874	2	4	5	40	0.5	0.9	1.126
2	5	1	40	0.9	0.1	1.196	2	5	1	40	0.9	0.1	0.934
3	1	3	60	0.1	0.5	0.682	3	1	3	60	0.1	0.5	1.15
3	2	4	60	0.3	0.5	0.882	3	2	4	60	0.3	0.5	0.953
3	3	5	60	0.5	0.9	0.743	3	3	5	60	0.5	0.9	0.618
3	4	1	60	0.5	0.1	1.017	3	4	1	60	0.5	0.1	0.712
3	5	2	60	0.9	0.3	0.875	3	5	2	60	0.9	0.3	0.921
4	1	4	80	0.1	0.5	1.057	**4**	**1**	**4**	**80**	**0.1**	**0.5**	**1.380**
4	2	5	80	0.3	0.9	1.173	4	2	5	80	0.3	0.9	0.919
4	3	1	80	0.5	0.1	0.886	4	3	1	80	0.5	0.1	1.012
4	4	2	80	0.5	0.3	0.641	4	4	2	80	0.5	0.3	0.863
4	5	3	80	0.9	0.5	1.174	4	5	3	80	0.9	0.5	1.06
5	1	5	100	0.1	0.9	0.965	5	1	5	100	0.1	0.9	0.817
5	2	1	100	0.3	0.1	0.982	5	2	1	100	0.3	0.1	1.066
5	3	2	100	0.5	0.3	1.258	5	3	2	100	0.5	0.3	0.926
5	4	3	100	0.5	0.5	1.095	5	4	3	100	0.5	0.5	0.703
5	5	4	100	0.9	0.5	0.624	5	5	4	100	0.9	0.5	0.621

accuracy assessment, samples were collected from field surveying in 2009 and reference maps from Jabatan Ukur Dan Pemetaan Malaysia (JUPEM). Confusion matrix can be used to conduct four types of accuracy assessments that are related to different aspects, and it can determine the overall accuracy, producer accuracy, user accuracy, and kappa coefficients [34]. Overall accuracy is measured as the total number of correctly classified pixels divided by the total number of test pixels. Producer accuracy is related to the probability that the specific land cover of an area is classified as such. User accuracy is associated with the probability that a pixel is accurately labeled as a certain land cover class in the map. Kappa coefficient is the difference of the actual agreement between the reference data and an automated classifier from the chance agreement between the reference data and a random classifier [50].

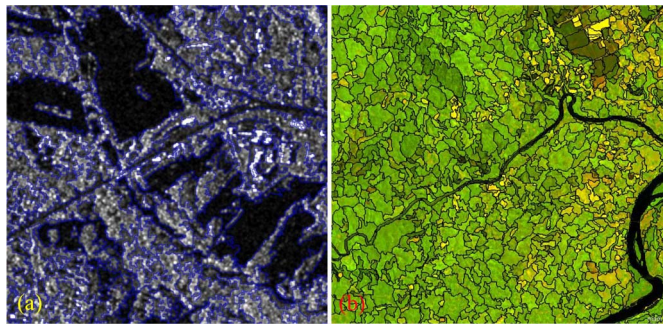

Fig. 3. Segmented (a) TerraSAR-X and (b) Landsat imagery.

IV. RESULTS

A. Optimization and Segmentation Results

As mentioned in the methodology section, 243 combinations can be defined using three parameters, namely, scale, color, and shape. The Taguchi optimization technique reduces the number of experiments reduced to 25, as shown in Table III. This table represents the experiments selected (available combinations) given the segmentation parameters and the measured POFs for each combination.

Table III suggests that the maximum POF (1.310) obtained for the TerraSAR-X image combined parameter values of 40, 0.1, and 0.3 for scale, color, and shape, respectively. By contrast, the maximum POF of 1.380 for the Landsat image combined parameter values of 80, 0.1, and 0.5 for scale, color, and shape, respectively. Thus, these two combinations are the optimum segmentation parameters for the two data sets. The generated segmentation maps are depicted in Fig. 3. Fig. 3(a) displays the segmentation of the entire Landsat scene; however, Fig. 3(b) displays only a small portion of the segmented TerraSAR-X image given its very high spatial resolution. This small region is presented for enhanced visualization because the segmented areas were very small and could not be observed from afar.

The optimum segmentation parameters determined using the Taguchi technique were used to recognize object boundaries with reasonable accuracy. The precision of this segmentation

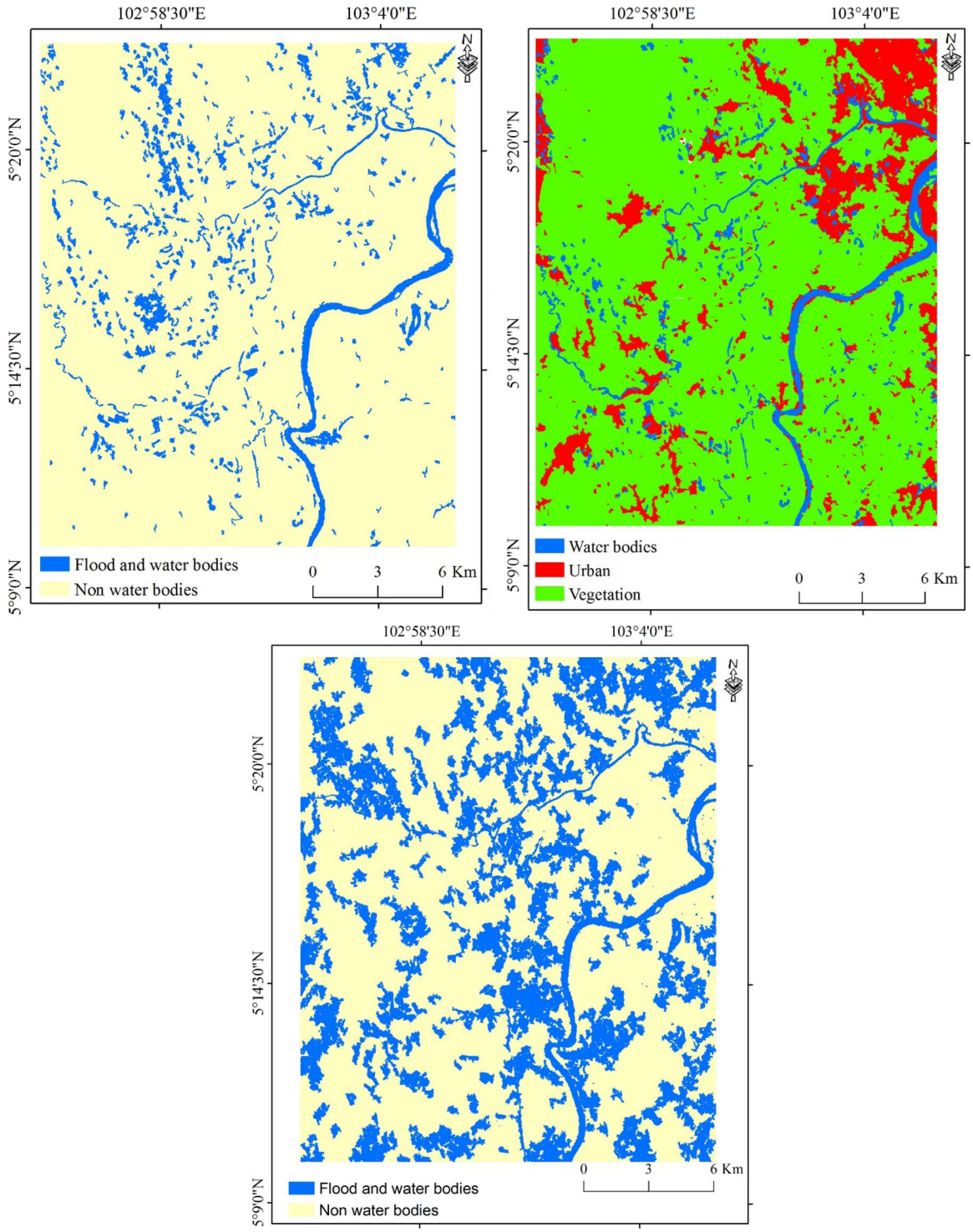

Fig. 4. Classified maps. (a) TerraSAR-X using the rule-based method. (b) Landsat imagery. (c) TerraSAR-X using the ISODATA method.

was assessed visually as the boundaries of most of the objects were detected accurately. The results also confirmed the efficiency of the multiresolution segmentation approach.

B. Classified Maps

The two images of TerraSAR-X and Landsat were classified according to the segmentation results and the defined rules. Fig. 4(a) illustrates the classified map of the TerraSAR-X image using the rule-based method, which contains two classes, namely, water and nonwater bodies. Fig. 4(b) depicts the classified map of Landsat imagery, which consists of three classes, i.e., urban, vegetation, and water. Furthermore, the classified TerraSAR-X map using ISODATA can be seen in Fig. 4(c).

The extent of the water bodies visualized in the classified Landsat image [Fig. 4(b)] was less than the amount of water bodies depicted in the TerraSAR-X image [Fig. 4(a)]. The water bodies detected in the classified TerraSAR-X map are

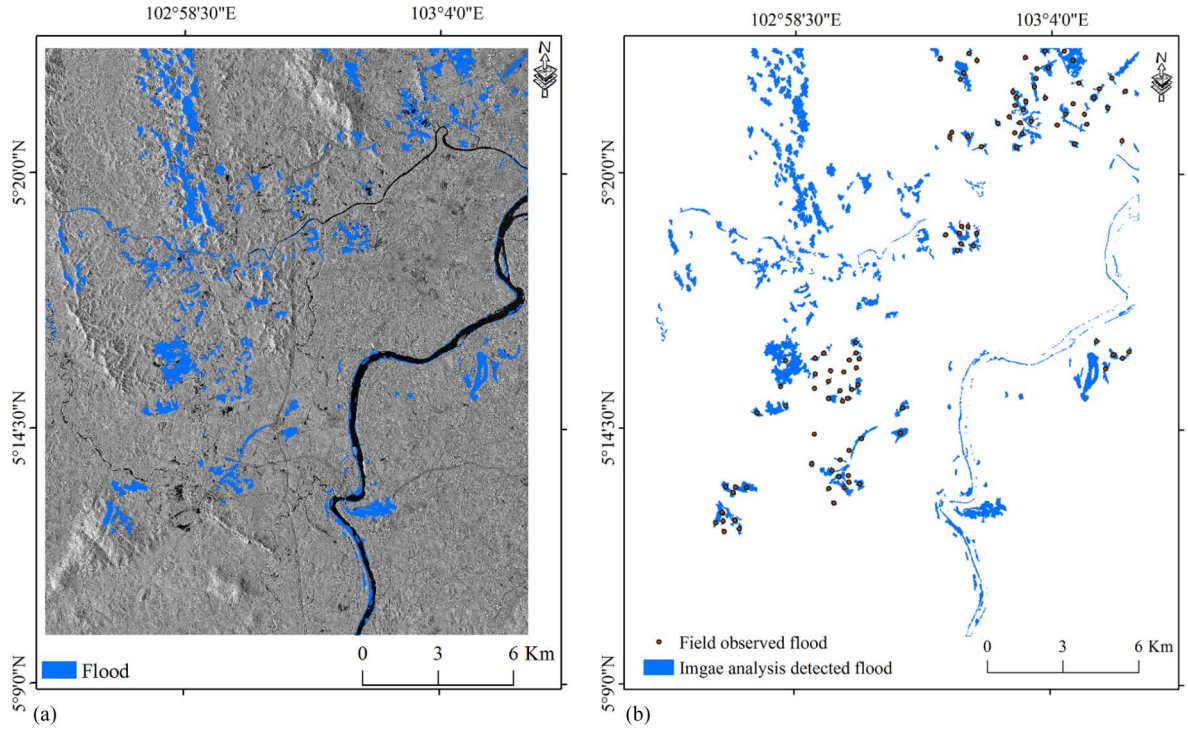

Fig. 5. (a) Hill-shaded map of the study area with flood locations that was detected by subtracting the classes of water bodies derived from both images. (b) Flooded areas without hill-shaded map.

TABLE IV
CONFUSION MATRIX FOR TERRASAR-X USING RULE BASED IN OBJECT-BASED CLASSIFICATION

Classes	Producer accuracy	User accuracy
Water bodies	93.08	91.92
Non water bodies	89.6	84.57
Overall accuracy	86.18	
Kappa coefficient	0.72	

TABLE V
CONFUSION MATRIX FOR TERRASAR-X USING ISODATA CLASSIFICATION

Classes	Producer accuracy	User accuracy
Water bodies	51.94	60.48
Non water bodies	55.27	51.98
Overall accuracy	57.98	
Kappa coefficient	0.41	

TABLE VI
CONFUSION MATRIX FOR LANDSAT

Classes	Producer accuracy	User accuracy
Water bodies	95.14	90.74
Vegetation	93.06	99.88
Urban	90.61	81.92
Overall accuracy	93.04	
Kappa coefficient	0.77	

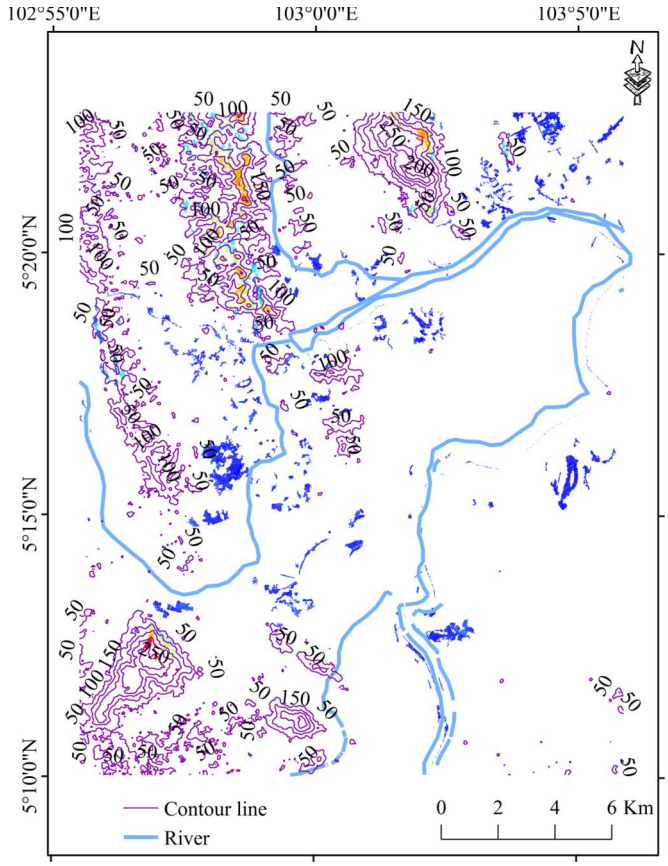

Fig. 6. Masked DEM using flooded locations.

flooded regions; by subtracting the two classified water bodies, we determined the locations of the flooded areas. As can be seen in Fig. 4(c), considerable misclassifications are evident in the result of ISODATA analysis. This observation shows the weakness of unsupervised methods in classification. The confusion matrix gives information about the precision of the

results. Fig. 5 illustrates the flood locations detected in the study area by the rule-based method as shown in Tables I and II.

A confusion matrix was generated to assess the efficiency of the proposed method and to evaluate the generated flood inventory map. Tables IV and V display the confusion matrix results for the classified maps of TerraSAR-X using the rule-based and ISODATA classification methods, respectively. Moreover, Table VI shows the confusion matrix results for Landsat images.

The overall accuracies of the classified maps of the TerraSAR-X and Landsat images were 86.18 and 93.04, respectively, thus indicating that the rule-based method efficiently discriminates between objects. As a result, an accurate classification map is produced. Moreover, the kappa coefficients were 0.72 and 0.77 for the TerraSAR-X and Landsat classified maps, respectively. Both accuracy assessment results suggest that all of the user and producer accuracy values are reasonably high, thereby suggesting that the generated classes are reliable. The flood location map was constructed by subtracting the two derived water bodies; thus, their accuracy values directly affect map precision. Statistically, 69% of the flood took place in the vegetation areas, and the rest happened in the urban areas. The confusion matrix indicated that both water bodies had high producer and user accuracy values, thus confirming the reliability of the final flood location map generated. However, the overall accuracy achieved by ISODATA was 57.98, which is considerably less than the acquired accuracy from the rule-based method.

V. Discussion

This study has presented an approach to overcome the difficulties in flood detection by combining Landsat (medium spatial resolution) and TerraSAR-X (high spatial resolution) imageries. The results of our study correspond with other works suggesting that Landsat data can be useful for water area extraction and mapping [51], [52]. Current research then extends previous studies on combination of various sensors for flood detection using optical and active sensors [53], [54].

The main rationale of using Landsat data in current study was to extract the water bodies before flooding. This can be done using many ways; however, the aim was to use purely spaceborne remote-sensing-based methods in a cost-effective way. The difference in the spatial resolution can be an issue. However, in this study, the accuracies acquired from both Landsat and TerraSAR-X classifications were reasonably similar, which proved that both datasets were applicable for such application.

In Fig. 5(a), several of the flooded locations were in hilly areas. Overlay analysis was conducted to assess the precision of the proposed flood detection method and the derived flood inventory. Elevation was masked using the detected flooded locations (Fig. 6). Most of the flooded areas were located in an elevation of 2–280 m. The elevation of the whole study area ranged between 0 and 1445 m.

TerraSAR-X could perform better than Landsat in classifying areas near rivers. The efficiency of TerraSAR-X in flood studies has been proven by current and various researches [55]. Misclassifications were visible in the Landsat image because of the segmentation process. For example, the existence of wetlands near the river or in the boundary of the river could be segmented as a water object. Moreover, Landsat showed misclassification in high-contrast areas such as a city with vegetation areas in the midst of urban spaces [56], [57]. TerraSAR-X works well in less dense vegetation areas because the radar's beam cannot penetrate through the vegetation [58], [59]. TerraSAR-X showed misclassification in urban and vegetation areas where buildings and long trees coexist [60].

The proposed method works reasonably well in open areas or regions without tall structures. Therefore, accurate classification can be obtained in rural areas, but accuracy will be reduced in urban areas partly because of the restricted visibility of TerraSAR-X of the ground surface owing to shadow and layover [33], [61]. The algorithm proposed by [62] proved that flooding in rural areas can be detected by TerraSAR-X with good accuracy and in urban areas with reasonable accuracy. The accuracy was reduced in urban areas partly because of TerraSAR-X's restricted visibility of the ground surface attributed to radar shadow and layover. This problem can be solved using another data source (e.g., such as airborne laser scanning data, i.e., LiDAR), where the area behind the tall feature can be modeled [33], [63], as proposed by [33]. However, obtaining airborne laser scanning data is a very expensive affair and not easily available for less developed countries. Another limitation of this method shows when the flooded areas are wetlands, such as farmlands where the differentiation between the flooded areas and the water for planting is difficult [64], [65].

The TerraSAR-X data used in the current research were HH polarized. Such polarization data are less affected by variations in water surface roughness caused by wind or vegetation compared to other polarization types [66]. Moreover, the HH-polarized backscattered coefficient generally presents a higher contrast between water and land surfaces [67]. Accuracy assessment showed that the rule-based method is significantly stronger than the unsupervised ISODATA method. Therefore, the proposed methodology is an easy, rapid, reliable, and low-cost procedure to map flood locations. Researchers may use this method to construct a flood inventory that will serve as basis for flood susceptibility, hazard, and risk analyses.

It has been shown that the accuracy of Landsat is limited if the object has less than two pixel size. This may cause some problems covering the small streams where it is the case in some parts of this study. Moreover, some other streams were too narrow to not be detected by both sensors. This can be one of the sources for some of the misclassification [15].

On the other hand, when comparing Landsat and TerraSAR-X classified results visually, the active sensor has less misclassification mostly due to the high spatial resolution and the high capability of the active sensor in detecting the water bodies. This statement has been proven by many studies which utilized SAR data to recognize the flood locations [68]–[71]. The shadow did not have a significant influence as most of the area is an open area. Moreover, even in the urban areas, there are no tall buildings that exist to create the problem

of shadow, which could enhance the result. This issue may be resolved by user interaction to correct some of the parts where it is a well-known area, but it is time-consuming.

When comparing the proposed method in this study to other studies, two published papers were considered. The first one is "Flood detection in urban areas using TerraSAR-X" authored by [33], and the second one is "The accuracy of sequential aerial photography and SAR data for observing urban flood dynamics, a case study of the UK summer 2007 floods" authored by [63]. In both of the aforementioned studies, the authors aimed to estimate the regions of the image in which water would not be visible due to shadow or layover caused by buildings. However, in the current case study, most of the area is flat (plain), and the buildings are not tall enough to make a considerable shadow effect.

Finally, in the current research, three issues can be highlighted: the complimentary use of freely downloadable optical Landsat data in flood studies, the segmentation process using the Taguchi algorithm, and the rule-based–object-based method. It is proved that Landsat has significant capability in this kind of research; however, the differences in the spatial resolutions made few misclassifications in the boundary of the water bodies such as river. On the other hand, the Taguchi method was very helpful in reducing the time required to employ all possible segmentation combinations as it reduced the number of possible combinations from 243 into 25 experiments. Finally, the rule-based object-based method performed better than the unsupervised classification ISODATA algorithm, although both were applied on the segmented data.

VI. Conclusion

Flood detection and inventory map production are very important in the assessment of natural hazards and in the prevention of flood in tropical areas. Some of the optical sensors cannot capture data effectively during flooding because of cloud cover. This limitation can be overcome by the introduction of very high resolution active sensors, which have revolutionized hazard studies. The current research developed an efficient flood mapping method to facilitate and enhance the application of traditional flood detection methods, some of which are time-consuming, are costly, and require much work. This study detected flooded areas precisely and rapidly using only two data sets and through a simple analysis. The state of Kuala Terengganu in Malaysia was selected as the test bed site because it frequently experiences flooding. The object-oriented rule-based classification method was used to extract the water bodies from TerraSAR-X data obtained during a flood event. Furthermore, Landsat imagery was captured prior to flood season, which denotes the period in which flooding did not occur in the study area. The water bodies from Landsat imagery were mapped using the same classification technique and were subsequently subtracted from the TerraSAR-X-derived water bodies. The remaining water bodies represented the flooded locations in the study area. The quality of the study was enhanced by the Taguchi optimization technique, multiresolution segmentation, and rule-based classification. These techniques also expedited the process. The ISODATA classification method was used to map the TerraSAR-X for comparison purposes. The precision and reliability of the proposed method were assessed by a confusion matrix, and the acquired accuracy values proved the applicability of the proposed method in flood inventory mapping. ISODATA was incapable of mapping the water bodies with acceptable accuracy. Thus, this method is not applicable in flood detection studies. Unsupervised methods do not use the characteristics of the object, such as texture and shape, in classification. The proposed rule-based method can be used in flood detection in tropical and nontropical areas with acceptable accuracy and reduced budget. Planners and researchers can therefore use the derived maps to study flood susceptibility, hazard, and risk mapping further.

Acknowledgment

The authors would like to thank the National Mapping Agency (JUPEM), Malaysia, for providing various datasets used in this paper. The German Aerospace Center (DLR) provided the TerraSAR-X data under the Science proposal ID:HYD0326.

References

[1] J. M. Martinez and T. Le Toan, "Mapping of flood dynamics and spatial distribution of vegetation in the Amazon floodplain using multitemporal SAR data," *Remote Sens. Environ.*, vol. 108, no. 3, pp. 209–223, 2007.

[2] A. M. Youssef, B. Pradhan, and A. M. Hassan, "Flash flood risk estimation along the St. Katherine road, southern Sinai, Egypt using GIS based morphometry and satellite imagery," *Environ. Earth. Sci.*, vol. 62, no. 3, pp. 611–623, 2011.

[3] M. S. Tehrany, B. Pradhan, and M. N. Jebur, "Spatial prediction of flood susceptible areas using rule based decision tree (DT) and a novel ensemble bivariate and multivariate statistical models in GIS," *J. Hydrol.*, vol. 504, no. 4, pp. 69–79, 2013.

[4] M. S. Tehrany, B. Pradhan, and M. N. Jebur, "Flood susceptibility mapping using a novel ensemble weights-of-evidence and support vector machine models in GIS," *J. Hydrol.*, vol. 512, no. 2, pp. 332–343, 2014.

[5] F. Ip *et al.*, "Flood detection and monitoring with the Autonomous Sciencecraft Experiment onboard EO-1," *Remote Sens. Environ.*, vol. 101, no. 4, pp. 463–481, 2006.

[6] B. Pradhan, U. Hagemann, M. Shafapour Tehrany, and N. Prechtel, "An easy to use ArcMap based texture analysis program for extraction of flooded areas from TerraSAR-X satellite image," *Comput. Geosci.*, vol. 63, no. 2, pp. 34–43, 2014.

[7] M. S. Tehrany, M. J. Lee, B. Pradhan, M. N. Jebur, and S. Lee, "Flood susceptibility mapping using integrated bivariate and multivariate statistical models," *Environ. Earth. Sci.*, vol. 72, no. 10, pp. 1–15, 2014. [Online]. Available: http://dx.doi.org/10.1007/s12665-014-3289-3.

[8] G. R. Brakenridge, E. Anderson, S. V. Nghiem, S. Caquard, and T. B. Shabaneh, "Flood warnings, flood disaster assessments, and flood hazard reduction: The roles of orbital remote sensing," in *Proc. 30th Int. Symp. Remote Sens. Environ.*, 2003, pp. 1–6.

[9] G. Schumann, P. D. Bates, M. S. Horritt, P. Matgen, and F. Pappenberger, "Progress in integration of remote sensing-derived flood extent and stage data and hydraulic models," *Rev. Geophys.*, vol. 47, no. 4, pp. 18–29, 2009.

[10] P. Farina, D. Colombo, A. Fumagalli, F. Marks, and S. Moretti, "Permanent scatterers for landslide investigations: Outcomes from the ESA-SLAM project," *Eng. Geol.*, vol. 88, no. 3, pp. 200–217, Dec. 2006.

[11] E. Opolot, "Application of remote sensing and geographical information systems in flood management: A review," *Res. J. Appl. Sci. Eng. Technol.*, vol. 5, no. 10, pp. 1884–1894, 2013.

[12] F. A. Hirpa *et al.*, "Upstream satellite remote sensing for river discharge forecasting: Application to major rivers in South Asia," *Remote Sens. Environ.*, vol. 131, no. 2, pp. 140–151, 2013.

[13] T. W. Gillespie, J. Chu, E. Frankenberg, and D. Thomas, "Assessment and prediction of natural hazards from satellite imagery," *Prog. Phys. Geog.*, vol. 31, no. 5, pp. 459–470, 2007.

[14] R. Oberstadler, H. Hönsch, and D. Huth, "Assessment of the mapping capabilities of ERS-1 SAR data for flood mapping: A case study in Germany," *Hydrol. Process.*, vol. 11, no. 10, pp. 1415–1425, 1997.

[15] K. Auynirundronkool *et al.*, "Flood detection and mapping of the Thailand Central plain using RADARSAT and MODIS under a sensor Web environment," *Int. J. Appl. Earth. Observ.*, vol. 14, no. 1, pp. 245–255, 2012.

[16] Y. Chambenoit, N. Classeau, E. Trouvé, and J. P. Rudant, "Performance assessment of multitemporal SAR images' visual interpretation," in *Proc. IEEE Int. Geosci. Remote Sens. Symp.*, 2003, pp. 3911–3913.

[17] J. Sanyal and X. Lu, "Application of remote sensing in flood management with special reference to monsoon Asia: A review," *Nat. Hazards.*, vol. 33, no. 2, pp. 283–301, 2004.

[18] M. Horritt, D. Mason, and A. Luckman, "Flood boundary delineation from synthetic aperture radar imagery using a statistical active contour model," *Int. J. Remote Sens.*, vol. 22, no. 13, pp. 2489–2507, 2001.

[19] M. Karjalainen, V. Kankare, M. Vastaranta, M. Holopainen, and J. Hyyppä, "Prediction of plot-level forest variables using TerraSAR-X stereo SAR data," *Remote Sens. Environ.*, vol. 117, no. 1, pp. 338–347, 2012.

[20] M. Horritt, D. Mason, D. Cobby, I. Davenport, and P. Bates, "Waterline mapping in flooded vegetation from airborne SAR imagery," *Remote Sens. Environ.*, vol. 85, no. 3, pp. 271–281, 2003.

[21] S. Elbialy, A. Mahmoud, B. Pradhan, and M. Buchroithner, "Application of spaceborne synthetic aperture radar data for extraction of soil moisture and its use in hydrological modelling at Gottleuba Catchment, Saxony, Germany," *J. Flood. Risk. Manag.*, vol. 7, no. 2, pp. 159–175, 2013.

[22] L. Pulvirenti, M. Chini, N. Pierdicca, L. Guerriero, and P. Ferrazzoli, "Flood monitoring using multi-temporal COSMO-SkyMed data: Image segmentation and signature interpretation," *Remote Sens. Environ.*, vol. 115, no. 4, pp. 990–1002, 2011.

[23] D. C. Mason, M. S. Horritt, J. T. Dall'Amico, T. R. Scott, and P. D. Bates, "Improving river flood extent delineation from synthetic aperture radar using airborne laser altimetry," *IEEE Trans. Geosci. Remote Sens.*, vol. 45, no. 12, no. 12, pp. 3932–3943, Dec. 2007.

[24] Y. Cunjian, W. Siyuan, Z. Zengxiang, and H. Shifeng, "Extracting the flood extent from satellite SAR image with the support of topographic data," in *Proc. Int. Conf. Info-tech. Info-net*, 2001, pp. 87–92.

[25] G. Nico, M. Pappalepore, G. Pasquariello, A. Refice, and S. Samarelli, "Comparison of SAR amplitude vs. coherence flood detection methods—A GIS application," *Int. J. Remote Sens.*, vol. 21, no. 8, pp. 1619–1631, 2000.

[26] M. N. Jebur, B. Pradhan, and M. S. Tehrany, "Detection of vertical slope movement in highly vegetated tropical area of Gunung pass landslide, Malaysia, using L-band InSAR technique," *Geosci. J.*, vol. 18, no. 1, pp. 61–68, 2013.

[27] B. Brisco, A. Schmitt, K. Murnaghan, S. Kaya, and A. Roth, "SAR polarimetric change detection for flooded vegetation," *Int. J. Digit. Earth.*, vol. 6, no. 2, pp. 103–114, 2013.

[28] M. S. Tehrany, B. Pradhan, and M. N. Jebu, "A comparative assessment between object and pixel-based classification approaches for land use/land cover mapping using SPOT 5 imagery," *Geocarto. Int.*, vol. 12, no. 2, pp. 1–19, 2013. [Online]. Available: http://dx.doi.org/10.1080/10106049.2013.768300.

[29] J. Chen, X. Zhu, J. E. Vogelmann, F. Gao, and S. Jin, "A simple and effective method for filling gaps in Landsat ETM+ SLC-off images," *Remote Sens. Environ.*, vol. 115, no. 4, pp. 1053–1064, 2011.

[30] C. Zhang, W. Li, and D. Travis, "Gaps-fill of SLC-off Landsat ETM+ satellite image using a geostatistical approach," *Int. J. Remote Sens.*, vol. 28, no. 22, pp. 5103–5122, 2007.

[31] V. Karathanassi, P. Kolokousis, and S. Ioannidou, "A comparison study on fusion methods using evaluation indicators," *Int. J. Remote Sens.*, vol. 28, no. 10, pp. 2309–2341, 2007.

[32] B. Aiazzi, S. Baronti, M. Selva, and L. Alparone, "MS + pan image fusion by an enhanced Gram-Schmidt spectral sharpening," in *Proc. 26th EARSeL Symp. "New Strategies Eur. Remote Sens.,"* 2007, pp. 113–120.

[33] D. C. Mason *et al.*, "Flood detection in urban areas using TerraSAR-X," *IEEE. Trans. Geosci. Remote Sens.*, vol. 48, no. 2, pp. 882–894, Feb. 2010.

[34] A. Hamedianfar and H. Z. Shafri, "Development of fuzzy rule-based parameters for urban object-oriented classification using very high resolution imagery," *Geocarto. Int.*, vol. 29, no. 1, pp. 1–25, 2013.

[35] M. N. Jebur, H. Z. Mohd Shafri, B. Pradhan, and M. S. Tehrany, "Per-pixel and object-oriented classification methods for mapping urban land cover extraction using SPOT 5 imagery," *Geocarto. Int.*, vol. 12, no. 2, pp. 1–15, 2013. [Online]. Available: http://dx.doi.org/10.1080/10106049.2013.848944.

[36] M. S. Tehrany, B. Pradhan, and M. N. Jebur, "Remote sensing data reveals eco-environmental changes in urban areas of Klang Valley, Malaysia: Contribution from object based analysis," *J. Indian. Soc. Remote Sens.*, vol. 41, no. 4, pp. 981–991, 2013.

[37] T. R. Martha, N. Kerle, C. J. van Westen, V. Jetten, and K. V. Kumar, "Segment optimization and data-driven thresholding for knowledge-based landslide detection by object-based image analysis," *IEEE. Trans. Geosci. Remote Sens.*, vol. 49, no. 12, pp. 4928–4943, Dec. 2011.

[38] S. Siyahghalati, A. K. Saraf, B. Pradhan, M. N. Jebur, and M. S. Tehrany, "Rule-based semi-automated approach for the detection of landslides induced by 18 September 2011 Sikkim, Himalaya, earthquake using IRS LISS3 satellite images," *Geomat. Nat. Haz. Risk.*, vol. 10, no. 2, pp. 1–19, 2014.

[39] V. Moosavi, A. Talebi, and B. Shirmohammadi, "Producing a landslide inventory map using pixel-based and object-oriented approaches optimized by Taguchi method," *Geomorphology*, vol. 204, no. 1, pp. 646–656, 2014.

[40] M. Horritt, "A statistical active contour model for SAR image segmentation," *Image. Vis. Comput.*, vol. 17, no. 3, pp. 213–224, 1999.

[41] A. Voisin, V. A. Krylov, G. Moser, S. B. Serpico, and J. Zerubia, "Classification of very high resolution SAR images of urban areas using copulas and texture in a hierarchical Markov random field model," *IEEE Geosci. Remote Sens. Lett.*, vol. 10, no. 1, pp. 96–100, Jan. 2013.

[42] G. Taguchi, *Introduction to Quality Engineering: Designing Quality Into Products and Processes*. White Plains, NY, USA: Quality Resources, 1986.

[43] C. Baker, R. Lawrence, C. Montagne, and D. Patten, "Mapping wetlands and riparian areas using Landsat ETM+ imagery and decision-tree-based models," *Wetlands*, vol. 26, no. 2, pp. 465–474, 2006.

[44] F. Zambon *et al.*, "Application of classification methods for mapping Mercury's surface composition: Analysis on Rudaki's area," in *Proc. EPSC-DPS Joint Meet.*, 2011, p. 782.

[45] D. Chakraborty, V. Chowdhary, D. Dutta, and J. Sharma, "Classification of high spatial resolution image using multi circular local binary pattern and variance," *Int. J. Electron. Commun. Comput. Eng.*, vol. 4, no. 6, pp. 1648–1654, 2013.

[46] B. J. Irvin, S. J. Ventura, and B. K. Slater, "Fuzzy and ISODATA classification of landform elements from digital terrain data in Pleasant Valley, Wisconsin," *Geoderma*, vol. 77, no. 2, pp. 137–154, 1997.

[47] M. Galli, F. Ardizzone, M. Cardinali, F. Guzzetti, and P. Reichenbach, "Comparing landslide inventory maps," *Geomorphology*, vol. 94, no. 3, pp. 268–289, 2008.

[48] D. C. Duro, S. E. Franklin, and M. G. Dubé, "A comparison of pixel-based and object-based image analysis with selected machine learning algorithms for the classification of agricultural landscapes using SPOT-5 HRG imagery," *Remote Sens. Environ.*, vol. 118, no. 1, pp. 259–272, 2012.

[49] S. W. Myint, P. Gober, A. Brazel, S. Grossman-Clarke, and Q. Weng, "Per-pixel vs. object-based classification of urban land cover extraction using high spatial resolution imagery," *Remote Sens. Environ.*, vol. 115, no. 5, pp. 1145–1161, 2011.

[50] W. Zhou, A. Troy, and M. Grove, "Object-based land cover classification and change analysis in the Baltimore metropolitan area using multitemporal high resolution remote sensing data," *Sensors*, vol. 8, no. 3, pp. 1613–1636, 2008.

[51] Y. Wang, J. Colby, and K. Mulcahy, "An efficient method for mapping flood extent in a coastal floodplain using Landsat TM and DEM data," *Int. J. Remote Sens.*, vol. 23, no. 18, pp. 3681–3696, 2002.

[52] Y. Wang, "Using Landsat 7 TM data acquired days after a flood event to delineate the maximum flood extent on a coastal floodplain," *Int. J. Remote Sens.*, vol. 25, no. 5, pp. 959–974, 2004.

[53] N. Kussul, A. Shelestov, and S. Skakun, "Grid system for flood extent extraction from satellite images," *Earth. Sci. Inf.*, vol. 1, no. 3/4, pp. 105–117, 2008.

[54] A. Demirkesen, F. Evrendilek, S. Berberoglu, and S. Kilic, "Coastal flood risk analysis using Landsat-7 ETM+ imagery and SRTM DEM: A case study of Izmir, Turkey," *Environ. Monit. Assess.*, vol. 131, no. 1–3, pp. 293–300, 2007.

[55] L. Giustarini *et al.*, "A change detection approach to flood mapping in urban areas using TerraSAR-X," *IEEE Trans. Geosci. Remote Sens.*, vol. 51, no. 4, pp. 2417–2430, Apr. 2013.

[56] F. Yuan, K. E. Sawaya, B. C. Loeffelholz, and M. E. Bauer, "Land cover classification and change analysis of the Twin Cities (Minnesota) Metropolitan Area by multitemporal Landsat remote sensing," *Remote Sens. Environ.*, vol. 98, no. 2, pp. 317–328, 2005.

[57] W. L. Stefanov, M. S. Ramsey, and P. R. Christensen, "Monitoring urban land cover change: An expert system approach to land cover classification of semiarid to arid urban centers," *Remote Sens. Environ.*, vol. 77, no. 2, pp. 173–185, 2001.
[58] Y. Yajima, Y. Yamaguchi, R. Sato, H. Yamada, and W.-M. Boerner, "POLSAR image analysis of wetlands using a modified four-component scattering power decomposition," *IEEE Trans. Geosci. Remote Sens.*, vol. 46, no. 6, pp. 1667–1673, 2008.
[59] N. Short *et al.*, "A comparison of TerraSAR-X, RADARSAT-2 and ALOS-PALSAR interferometry for monitoring permafrost environments, case study from Herschel Island, Canada," *Remote Sens. Environ.*, vol. 115, no. 12, pp. 3491–3506, 2011.
[60] D. Brunner, L. Bruzzone, and G. Lemoine, "Change detection for earthquake damage assessment in built-up areas using very high resolution optical and SAR imagery," in *Proc. IEEE IGARSS*, 2010, pp. 3210–3213.
[61] D. C. Mason, L. Giustarini, J. Garcia-Pintado, and H. L. Cloke, "Detection of flooded urban areas in high resolution synthetic aperture radar images using double scattering," *Int. J. Appl. Earth. Observ.*, vol. 28, no. 2, pp. 150–159, 2014.
[62] D. C. Mason, I. J. Davenport, J. C. Neal, G. P. Schumann, and P. D. Bates, "Near real-time flood detection in urban and rural areas using high-resolution synthetic aperture radar images," *IEEE Trans. Geosci. Remote Sens.*, vol. 50, no. 8, pp. 3041–3052, Aug. 2012.
[63] G. J. P. Schumann, J. C. Neal, D. C. Mason, and P. D. Bates, "The accuracy of sequential aerial photography and SAR data for observing urban flood dynamics, a case study of the UK summer 2007 floods," *Remote Sens. Environ.*, vol. 115, no. 10, pp. 2536–2546, 2011.
[64] F. M. Henderson and A. J. Lewis, "Radar detection of wetland ecosystems: A review," *Int. J. Remote Sens.*, vol. 29, no. 20, pp. 5809–5835, 2008.
[65] P. Townsend, "Relationships between forest structure and the detection of flood inundation in forested wetlands using C-band SAR," *Int. J. Remote Sens.*, vol. 23, no. 3, pp. 443–460, 2002.
[66] V. Herrera-Cruz, F. Koudogbo, and V. Herrera, "TerraSAR-X rapid mapping for flood events," in *Proc. Int. Soc. Photogramm. Rem. Sens., Earth Imaging Geospatial Inf.*, 2009, pp. 170–175.
[67] J. B. Henry, P. Chastanet, K. Fellah, and Y. L. Desnos, "Envisat multi-polarized ASAR data for flood mapping," *Int. J. Remote Sens.*, vol. 27, no. 10, pp. 1921–1929, 2006.
[68] R. Hostache *et al.*, "Water level estimation and reduction of hydraulic model calibration uncertainties using satellite SAR images of floods," *IEEE Trans. Geosci. Remote Sens.*, vol. 47, no. 2, pp. 431–441, Feb. 2009.
[69] S. Martinis *et al.*, "Comparing four operational SAR-based water and flood detection approaches," *Int. J. Remote Sens.*, vol. 36, no. 13, pp. 3519–3543, 2015.
[70] C. Kuenzer *et al.*, "Varying scaule and capability of Envisat ASAR-WSM, TerraSAR-X ScanSAR and TerraSAR-X stripmap data to assess urban flood situations: A case study of the Mekong delta in Can Tho province," *Remote Sens.*, vol. 5, no. 10, pp. 5122–5142, 2013.
[71] C. Kuenzer, J. Huth, S. Martinis, L. Lu, and S. Dech, *SAR Time Series for the Analysis of Inundation Patterns in the Yellow River Delta, China*. New York, NY, USA: Springer-Verlag, 2015, pp. 427–441.

Biswajeet Pradhan received the B.Sc. degree (with honors) from Berhampur University, Berhampur, India, the M.Sc. degree from the Indian Institute of Technology (IIT), Bombay, India, the M.Tech. degree in civil engineering from the IIT, Kanpur, India, and the Dresden University of Technology, Dresden, Germany, the Ph.D. degree in GIS and geomatics engineering from the Universiti Putra Malaysia, Serdang, Malaysia, and the Habilitation in "remote sensing" from the Dresden University of Technology, in 2011.

From 2008 to 2010, he was a recipient of the Alexander von Humboldt Research Fellowship from Germany. He is currently a faculty member of the Department of Civil Engineering, Universiti Putra Malaysia. He has more than 16 years of teaching, research, consultancy, and industrial experience. Out of his more than 330 articles, more than 240 have been published in Science Citation Index (SCI/SCIE) technical journals. He has written 2 books on GIS data compression and disaster management, edited 3 volumes, and written 12 book chapters. He is on the editorial board of many ISI journals. He specializes in remote sensing, GIS application, and soft-computing techniques in natural hazard and environmental problems.

Dr. Pradhan was the recipient of the prestigious German Academic Exchange Research (DAAD) fellowship award, Saxony State Fellowship from 1999 to 2002, Keith Aurtherton Research Award, and Georg Forster Research Award from the German Government. Since March 2016, Professor Pradhan is serving as "Ambassador Scientist" for Alexander von Humboldt Foundation, Germany.

Mahyat Shafapour Tehrany was born in Tehran, Iran, on July 29, 1985. She received the B.Sc. degree from the Allameh Mohaddes Nouri, Mazandaran, Iran, in 2007, the M.Sc. degree from the Universiti Putra Malaysia, Serdang, Malaysia, in 2013, and the Ph.D. degree in GIS and geomatics engineering from the Universiti Putra Malaysia, in 2015.

Her areas of interest are flood, landslides, and ensemble modeling applications.

Mustafa Neamah Jebur was born in Misan, Iraq, on January 11, 1988. He received the B.Sc. degree from the Allameh Mohaddes Nouri, Mazandaran, Iran, in 2007, the M.Sc. degree from the Universiti Putra Malaysia, Serdang, Malaysia, in 2013, and the Ph.D. degree in GIS and geomatics engineering from the Universiti Putra Malaysia in 2015.

His areas of interest are flooding, landslides, and ensemble modeling applications.